Desalination and Water Treatment
www.deswater.com

doi:10.5004/dwt.2019.24462

165 (2019) 321–332
October

Photocatalyzed degradation of acid orange 7 dye under sunlight and ultraviolet irradiation using Ni- doped ZnO nanoparticles

Meghdad Pirsaheb[a], Kaveh Karimi[b,c], Behzad Shahmoradi[d], Masoud Moradi[a], Yasser Vasseghian[a,*], Elena Niculina Dragoi[e]

[a]*Research Center for Environmental Determinants of Health (RCEDH), Health Institute, Kermanshah University of Medical Sciences, Kermanshah, Iran, Tel. +989123446880, email: mpirsaheb@yahoo.com (M. Pirsaheb), Tel. +989183859910, email: mahfooz60@gmail.com (M. Moradi), Tel. +98 9183102214, email: yasser.vasseghian@kums.ac.ir, y_vasseghian@yahoo.com (Y. Vasseghian)*
[b]*Student Research Committee, Kermanshah University of Medical Sciences, Kermanshah, Iran, Tel. +989183786151, email: karimi6@gmail.com (K. Karimi)*
[c]*Water and Wastewater Kurdistan Company, Saghez, Iran*
[d]*Environmental Health Research Center, Research Institute for Health Development, Kurdistan University of Medical Sciences, Sanandaj, Iran, Tel. +989187705355, email: bshahmorady@gmail.com (B. Shahmoradi)*
[e]*Faculty of Chemical Engineering and Environmental Protection "CristoforSimionescu", "Gh. Asachi" Technical University, Iasi, BldMangeron no 73, 700050, Romania, Tel. +40 773719728, email: elenan.dragoi@gmail.com (E.N. Dragoi)*

Received 29 August 2018; Accepted 27 May 2019

ABSTRACT

The aim of this study was to evaluate the removal of acid orange 7 (AO7) dye using NiO doped ZnO nanoparticles under sunlight and ultraviolet (UV) irradiation. The characterization of catalyst was carried out via FTIR, SEM, XRD and XPS techniques. The result of XPS revealed that nickel was successfully incorporated in the ZnO matrix. In addition, artificial neural networks (ANN) were used to model the process and to generate useful predictions. A significant prediction model with R^2 of 0.991 and adjusted R^2 of 0.991 for sunlight Irradiation and with R^2 of 0.981 and adjusted R^2 of 0.980 for ultraviolet Irradiation were obtained from ANN. The obtained data indicated that there is a significant difference between the type of nanoparticles used in the dye removal. The dose of 0.8 g/l over a detention time of 90 min was able to remove 77% of the dye under sunlight and 93% under ultraviolet irradiation. The results showed that the synthesized nanoparticles could be utilized to photocatalytically degrade the dye at sunlight or using a UV lamp. Alhough there was a slight difference between the decomposition of this dye under sunlight and UV irradiation, using visible light at larger scale is more economical and generates less operational problems than UV light.

Keywords: Acid Orange 7; Nanocatalyst; Photocatalytic; Dye; Sunlight; Ultraviolet; Artificial neural network

1. Introduction

The textile dyeing industry generates large quantities of colored waste waters and therefore is a high source of pollution for clean water [1]. More than 15% of dyes are produced in various processes of textile manufactures, contributing thus to the generation of colored wastewater flows [2,3]. In addition, other industries such as pharmacy, food factories, cosmetics, paper mills, leather factorys, etc. contribute to this problem [4]. A large percentage of organic compounds identified in the water resources are chemical dyes, which come from both home and industry [5]. Dye materials not solely give the water an unpleasant appearance, but in some cases are very harmful and can gener-

*Corresponding author.

ate highly toxic byproducts via oxidation, hydrolysis or chemical reactions in water [6]. The presence of chemical dyes prevents the penetration of sunlight and causes the depletion of dissolved oxygen, fact which seriously affects the living organisms and the surrounding environment [7]. The dyes mainly consist of one or more poly cyclic benzene that cannot be completely removed from effluent and it is discharged into the environment as hazardous toxic waste; in turn, due to their toxicity and slow decomposition, they create an adverse effect on the surrounding environment [8–10]. Consequently, it is crucial to decrease pollution using suitable and feasible techniques [1].

There are various methods for treating color wastewater, among which we can enumerate conventional biological wastewater treatments systems, physical and chemical methods such as coagulation, filtration, activated carbon adsorption, irradiation, and membrane filtration [11]. They can be applied solely or in combination with biological processes. The biological processes are helpless for nonbiodegradable compounds removal whereas photodegradation (using suitable nanocatalysts) could be applied through utilizing a proper light source [12,13]. In the recent years, the photocatalytic processes were considered for decomposing harmful organic compounds, and, in this regard, TiO_2 and ZnO nanoparticles have been identified as the most promising photocatalysts [14]. Treating wastewater by nanophotocatalyst is an effective alternative method in the wastewater treatment to remove living organisms and organic matters simultaneously [15,16]. It can be stated that the free energy of photocatalytic reaction cell can remove micro-organisms, biodegradable and nonbiodegradable compounds. Due to the recycle of photocatalysts, this process is a cost-effective method [17]. Also, in terms of removing color from effluent in the presence of sunlight, fabricated nanophotocatlysts nanocrystals without any agglomeration and with the suitable size range for photodegradation (metal oxid-edoped ZnO nanoparticles) have a higher performance than undoped ZnO [18]. Therefore, metal oxide doped ZnO nanoparticles could be a suitable candidate for photodegradation of environmental pollutants including dyes [19]. The previous study confirmed that NiO doped ZnO through generation of radicals can degradation of organic pollutants as follows [20]:

$$\frac{\mathrm{NiO}}{\mathrm{ZnO}} + \mathrm{h}\vartheta \rightarrow \mathrm{e}^{-}\left(\mathrm{ZnO}\right) + \mathrm{h}^{+}\left(\mathrm{NiO}\right) \quad (1)$$

$$\mathrm{e}^{-} + \mathrm{O}_2 \rightarrow \mathrm{O}_2^{\bullet -} \quad (2)$$

$$\mathrm{h}^{+} + \mathrm{OH}^{-} \rightarrow {}^{\bullet}\mathrm{OH} \quad (3)$$

$$\mathrm{O}_2^{\bullet -} + \mathrm{H}_2\mathrm{O} \rightarrow \mathrm{HO}_2^{\bullet} + \mathrm{OH}^{-} \quad (4)$$

$$ROS + AO7 \rightarrow\rightarrow CO_2 + H_2O \quad (5)$$

In recent years, researchers have paid great attention to surface modification of ZnO with metals such as TiO_2 [21], Al [22,23], Ag [24,25], Cu [26], Cr [27], Mn [28], Li [29], Sn [30,31] and Fe [32]. These studies also showed that the above mentioned metals can alter the ZnO band gap energy and control the size of particles.

ZnO is an n-type semiconductor and its doping with NiO p-type semiconductor can alter its band gap energy and enhance the efficiency of this semiconductor in order to utilize the sun light in pollutants decomposition. In addition, use of suitable surface modifiers such as *n*-butylamine can reduce the size of nanoparticles. Hydrothermal synthesis is also preferred to other synthesis methods due to some advantages such as cost effectiveness, morphology control, and eco-friendliness of the process [33]. In a previous study by the authors, the neodymium-doped ZnO nanoparticles was synthesized using *n*-butylamine, as a surface modifier, under mild hydrothermal condition and yielded nanocrystals with an optimal size range without agglomeration and optical dispersion [34].

The purpose of this study was to evaluate the removal of AO7 dye using NiO-doped ZnO nanoparticles under sunlight and UV irradiation. The influence of effective photocatalytic parameters on the efficiency of nanoparticles such as type of nanoparticles (3 types), nanoparticles dosage, detention time, pH and different dye concentrations for decomposing AO7 under sunlight and UV irradiation was investigated. Table 1 explains the AO7 photocatalytic degradation results in previous studies.

Furthermore, in this study, AO7 removal efficiency using using Ni- doped ZnO nanoparticles under sunlight and ultraviolet irradiation modeled using ANN approach. To the author's knowledge, the AO7 dye removal has never been investigated using NiO-doped ZnO nanoparticles under sunlight and UV irradiation, this representing the novel aspect of the paper.

2. Materials and methods

2.1. Synthesis of Ni-doped nanocatalyst

In order to synthesize the selected nanoparticles, a specified amount of ZnO (1 mole) and dopent, NiO, of different percentages (0.5–1.5 mole %) were mixed together using NaOH as solvent under mild hydrothermal condition. 1 M commercial ZnO was taken as the starting precurse and then the dopant was added. For adjusting pH, affirm amount of 1 N HCl/NH_4OH was added. Then, *n*-butylamine (1 ml) was added to the prepared mixture, vigorously stirred for a few minutes. Finally, the mixture was moved to a teflon liner. Afterward, prepared samples were placed in a General Purpose autoclave (V_{fill} = 25 ml). The assembled autoclave was kept in an oven at a temperature of 100°C for 12 h. After running experiments, the product was rinsed with double distilled water. Later, the product was allowed to settle down and centrifuged at 3500 rpm for 15 min. Consequently, the synthesized nanoparticles were recovered and dried in an oven at 40–50°C for a few hours [41]. Dried particles were subjected to characterization as follow: functional groups related to catalyst surface were determined by Fourier-transform infrared spectroscopy (FTIR, FTS-165, BIO-RAD, USA). The x-ray diffraction technique (XRD, Quanta chrome, NOVA 2000) was employed for evaluation the crystal structure. The identification of surface composition was conducted by X-ray photoelectron spectroscopy (XPS, AXIS 165 (Kratos)). Scanning electron

Table 1
The results of the AO7 photocatalytic degradation in the literature

Authors	Photocatalyst	Light intensity	AO7 concentration	Photocatalyst dosage (g)	Removal (%)	Ref.
Sharma et al.	TiO_2	30 W/m²	50 mg/L	1 g/L	76	[35]
Han et al.	Fe-TiO_2	400 W/m²	50 mg/L	100 mg/L	96	[36]
Umukoro et al.	Pd-ZnO-exfoliated graphite	–	20 mg/L	0.1 g	87	[37]
Khani et al.	Immobilized nano ZnO on perlite Zinc Oxide Nanostructure	0.4 k Lux	15–55 mg/L	5 g/L	74	[38]
Akhlaghi	Prepared with Activated Carbon	400 W	10 mg/L	10 mg/L	80	[39]
Daneshvar et al.	UV/ZnO H_2O_2	0.55 kLux	20 mg/L	160 mg/L	90	[40]

microscope (SEM; Philips XL30) was used to survey of surface morphology.

2.2. Photodegradation experiments using nickel doped nanoparticles

The treatment capability (photodegradation) of synthesized nanoparticles was examined using AO7 (Fig. 1). The photoreactor characterization was mentioned with detail in the previous study [42]. Briefly, the reactor was made with 1.5 L capacity. In order to prevent short circuit, the input was designed at the bottom and the output at the top of the reactor. In order to establish continuous current, peristaltic pumps were employed (BT-100 1 L Longer pump, China). Also, the UV intensity was selected 20 W/m² (Fig. 2).

A Stock solution was prepared using AO7 dye (Sigma-Aldrich, Germany). This dye involves double bond of nitrogen (-N = N-) which connects two aromatic rings. Therefore, it could be harmful to human health, it is essential to formulate an appropriate method to remove it from water and wastewater. Then, the required concentrations were obtained from the stock solution and a certain amount of synthesized nanoparticles was added. After a certain time, the performance of the nanoparticles was analyzed.

2.3. Data analysis

The efficiency of nanoparticles and the effect of the parameters on dye removal were evaluated. The parameters investigated were nanoparticle types (0.5, 1, and 1.5 M% NiO), nanoparticle dosage (0.0–1.2 g/l), detention time (30, 60, and 90 min), light source (visible and UV), and pH (2–11). A certain amount of synthesized nanoparticles was added to different concentrations of dye. In order to achieve absorption-desorption equilibrium using a shaker, the mixture was placed under absolute darkness for at least 30 min at 50 rpm. Thereafter, each sample was separately subjected to sunlight and UV irradiation for 30–90 min. All the experiments under sunlight were carried out in an open area at 11:30 a.m. to 13 p.m. at 38 ± 3°C. Consequently, the dye concentration of each sample was determined using spectrophotometer (JENWAY 6305, England) at 484 nm (λ_{max} of AO7). Photocatalytic efficiency was calculated using Eq. (6):

$$R(\%) = 1 - \frac{c}{c_0} * 100 \quad (6)$$

where C_0 is the concentration of AO7 before radiation and C is the concentration of AO7 after radiation.

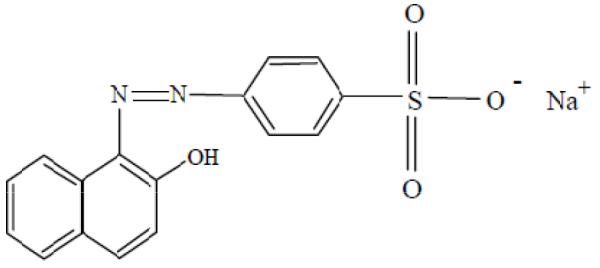

Fig. 1. Molecular structure of AO7 [32].

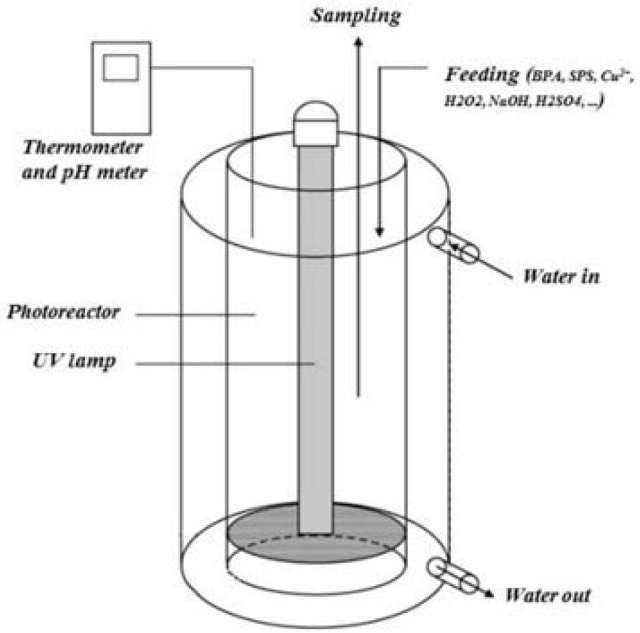

Fig. 2. Reactor picture.

2.4. Artificial neural network (ANN)

In this study, a forward feed ANN was trained by the back propagation approach with a hidden layer in the MATLAB software [44]. First, all experimental data were normalized by Eq. (7):

$$x = \frac{X_i - X_{min}}{X_{max} - X_{min}} \tag{7}$$

where X_i is the actual value of data for each input and output, X_{min} and X_{max} are the maximum and minimum values for each input and output, respectively and x is the normalized value of X_i. 24 data were randomly divided into three subset of training (16 data), validation (4 data) and testing (4 data). The training data was used to update the weights and biases using the Levenberge-Marquardt algorithm and the testing data were used to measure the network generalization capability. Also, validation data errors were monitored during training to prevent over fitting [45]. The transfer functions of tan-sigmoid (tansig) and linear (purelin) were selected for hidden and output layers, respectively. The number of neurons in the input and output layer was 4 (nanoparticles dosage, detention time, pH and dye concentration and 1 (dye removal), respectively. The number of neurons in the hidden layer was optimized by trial-and-error based on the mean square error (MSE) between the experimental and predicted values [45].

$$\mathrm{MSE} = \frac{1}{N}\sum_{i=1}^{N}\left(y_{i,\mathrm{pred}} - y_{i,\mathrm{exp}}\right)^2 \tag{8}$$

where N is the number of data points, $y_{i,pred}$ is the network prediction, $y_{i,exp}$ is the experimental response, and i is the index of the data point.

Each topology repeats 10 times to avoid random correlations for random weight and bias initialization [46,47]. In order to determine the accuracy of the model was calculated R^2, $R^2_{adj.}$, RMSE, MAE, AAD according to Eqs. (9)–(13) [35].

$$\mathrm{R}^2 = 1 - \left(\frac{\sum_{i=1}^{N}\left(y_{i,\mathrm{pred}} - y_{i,\mathrm{exp}}\right)^2}{\sum_{i=1}^{N}\left(y_{i,\mathrm{exp}} - y_{i,\mathrm{m}}\right)^2}\right) \tag{9}$$

$$\mathrm{R}^2_{\mathrm{adj.}} = 1 - \left(\left(1 - R^2\right)\frac{N-1}{N-K-1}\right) \tag{10}$$

$$\mathrm{RMSE} = \left(\frac{\sum_{i=1}^{N}\left(y_{i,\mathrm{pred}} - y_{i,\mathrm{exp}}\right)^2}{N}\right)^{1/2} \tag{11}$$

$$\mathrm{MAE} = \frac{1}{N}\left(\sum_{I=1}^{N}\left|y_{i,\mathrm{pred}} - y_{i,\mathrm{exp}}\right|\right) \tag{12}$$

$$\mathrm{AAD} = \frac{1}{N}\left(\sum_{I=1}^{N}\frac{\left|y_{i,\mathrm{pred}} - y_{i,\mathrm{exp}}\right|}{y_{i,\mathrm{exp}}}\right) \tag{13}$$

where N is the number of data points, K is the number of input variables, $y_{i,pred}$ is the network prediction, $y_{i,exp}$ is the experimental response, $y_{i,m}$ is the average of experimental response and i is the index of the data point.

3. Results and discussion

3.1. ANN modeling

One of the most important steps in the ANN model is to select the number of hidden layers and the number of neurons in the hidden layer [48,49]. The few number of neurons in the hidden layer leads to the performance of the network will not be satisfactory and a many number of neurons in the hidden layer leads to over fitting [50–52]. The optimal number of neurons in the hidden layer based on the mean square error (MSE) for sunlight and ultraviolet irradiation is presented in Figs. 3 and 4, respectively.

As shown in Figs. 3 and 4, the optimal topology for sunlight and ultraviolet irradiation is 4-8-1 and 4-7-1, respectively. The coefficient of determination between the experimental and predicted values for training, validation, test and all data in for sunlight and ultraviolet irradiation is shown in Figs. 5 and 6, respectively. The results of model' accuracy are presented in Table 2. As seen in Table 2, the high values of R^2 and $R^2_{adj.}$ represent a good agreement between the experimental and predicted values by

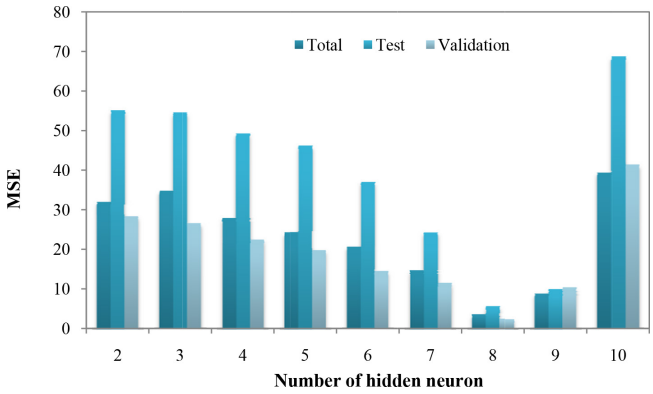

Fig. 3. Determination of optimum number of neurons for sunlight irradiation.

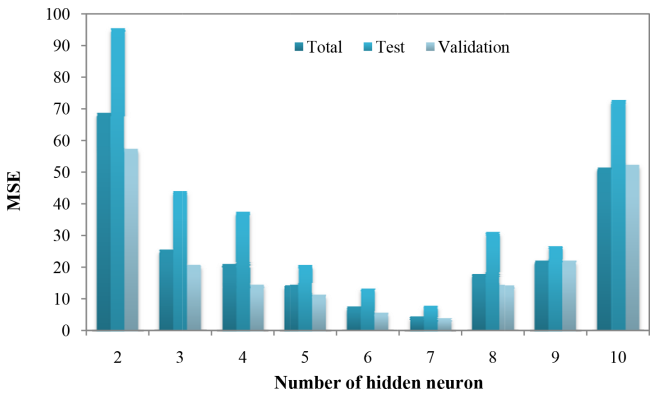

Fig. 4. Determination of optimum number of neurons for ultraviolet irradiation.

Table 2
Evaluation of the accuracy of ANN model

Factors	Sunlight irradiation	Ultraviolet irradiation
	(4-8-1)	(4-7-1)
R^2	0.991	0.981
R^2_{adj}	0.991	0.980
RMSE	2.350	2.783
MAE	1.630	1.499
AAD	0.0317	0.0234

the model. Also, the small values of RMSE, MAE and AAD indicate that the forecast error of the models is low and the models have good estimated characteristics.

3.2. Characterization results of nicled doped ZnO nanoparticles

3.21. XRD analysis

Nickel doped ZnO nanoparticles were successfully synthesized under hydrothermal conditions in the presence of *n*-butyl a mine as surface modifier, This surface modifier has low toxicity, cost effective, and result in low agglomeration of nanoparticles. Fig. 7 illustrates the strong and sharp peaks which indicated the proper cristalinity of nanoparticle. The peaks at 32°, 34.6°, 36.5°, 47.8°, 56.8°, 63° and 66.7° were appear in all patterns which are contributed to the lattice planes 010, 002, 001, 012, 110, 013 and 020 respectively [53]. Since the peak related to Ni appear at = 42–43° (lattice plane = 200), herein, the peaks of NiO were not observed that suggested nickel oxide is placed in the ZnO lattice [54].

Pascariu et al. investigated adding Ni and Co as dopant to the ZnO nanoparticles. They presented the XRD characteristic patterns by sol-gel method. They from these patterns observed all samples are polycrystalline. They found Ni and Co doped ZnO nanoparticles that sinthesized by co-precipitation method, able to improved photocatalytic activity in degradation of rhodamine B [55]. Liu et al. studied adding Copper as dopant to the ZnO lattice. They compared the Cu-doped ZnO and pure ZnO powders were synthesized by sol–gel method. Their results demonstrate that copper ions were well unified into the ZnO lattices by swaping Zn sites without changing the wurtzite structure and no secondary phase existed in Cu-doped ZnO nanoparticles [56].

3.2.2. SEM analysis

Morphology of the nanoparticles synthesized was studied using SEM. Characteristic SEM images show that the nanoparticles fabricated have kept their hexagonal structure (Fig. 8). However, the *n*-butylamine used as surfactant had no significant effect on the morphology or reducing agglomeration. Fig. 8b reveales the coupling between NiO and ZnO was increased by raising of Ni loading [57]. Moreover, the particle size was

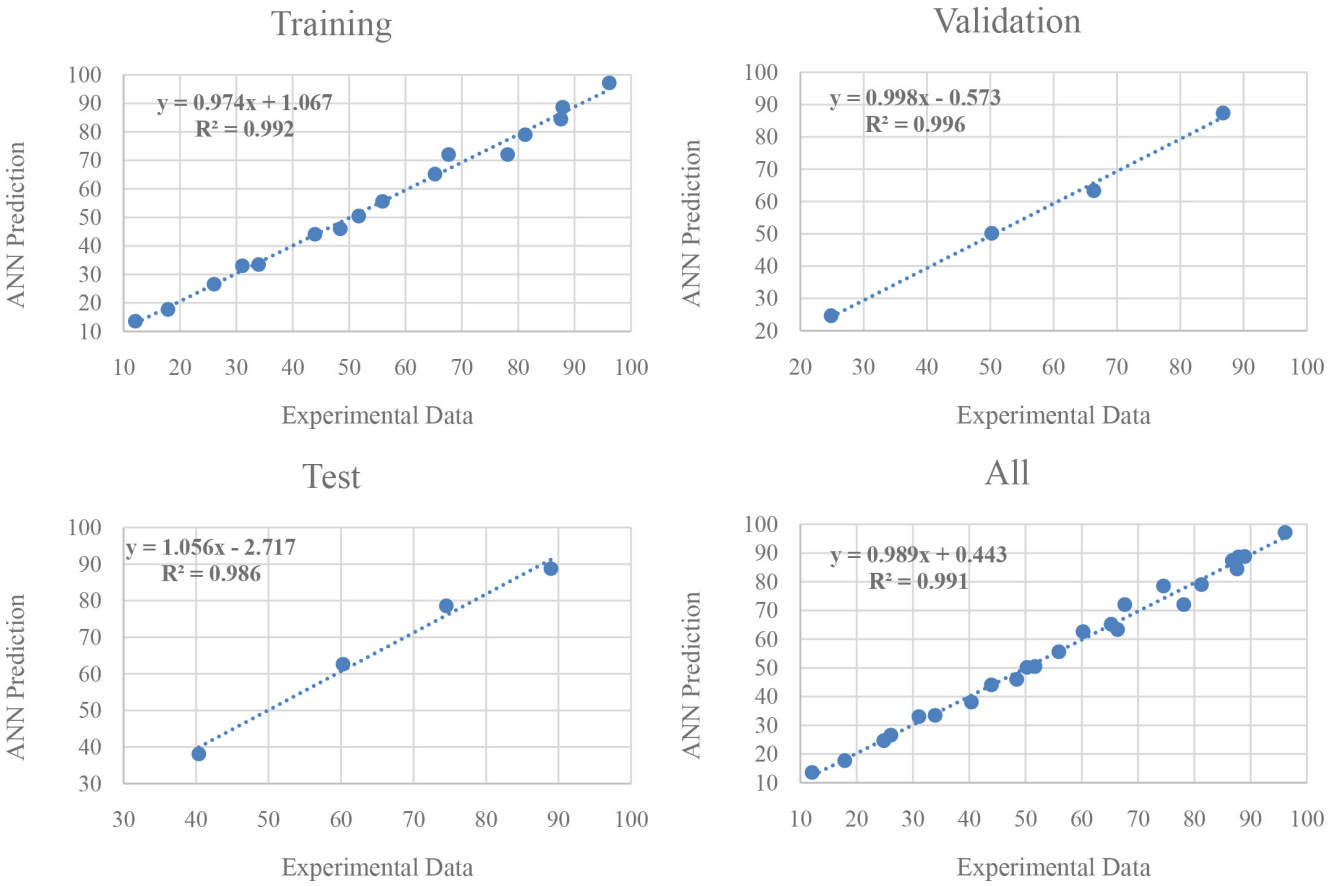

Fig. 5. Neural network model with training, validation, test and all prediction set for sunlight irradiation.

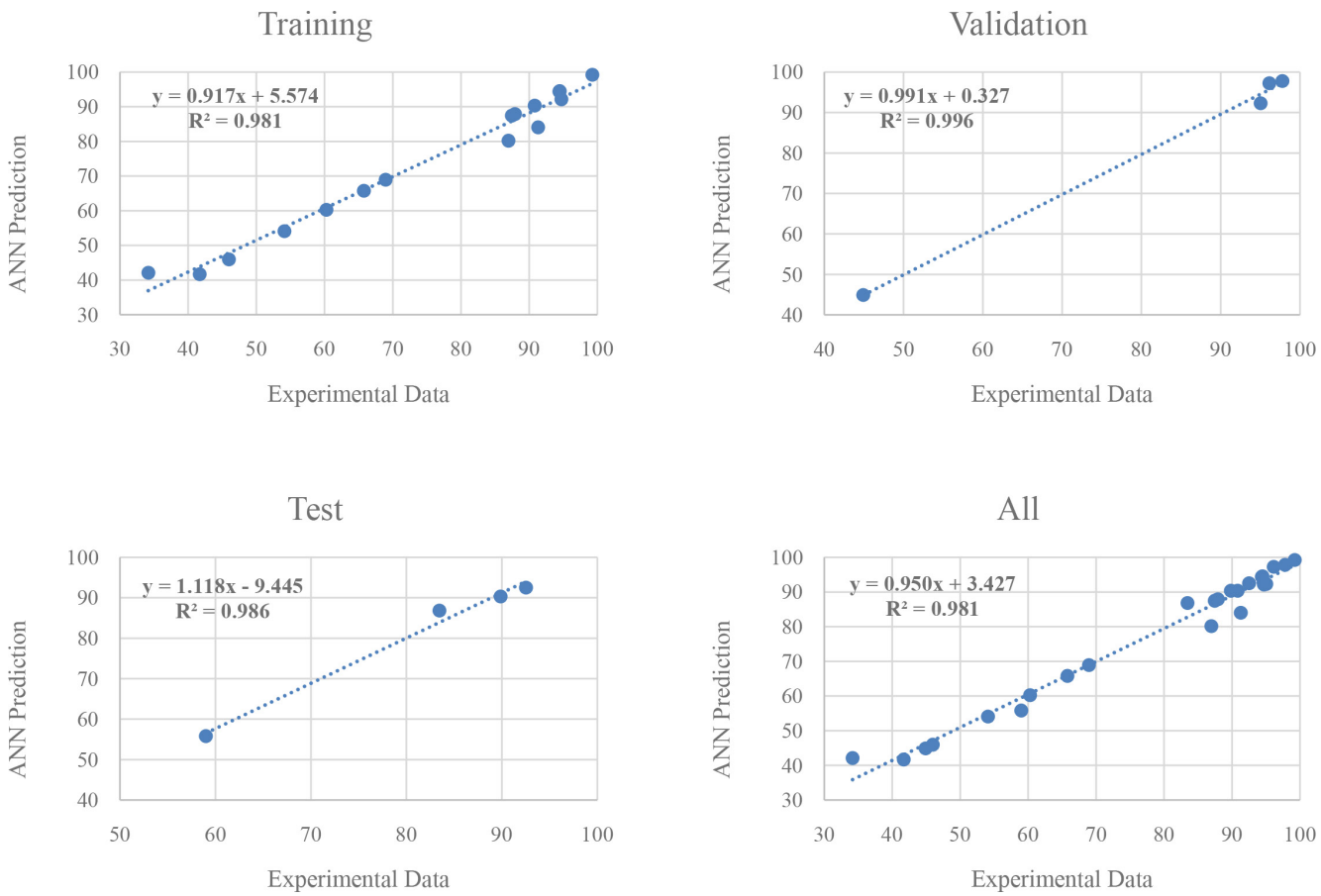

Fig. 6. Neural network model with training, validation, test and all prediction set for ultraviolet irradiation.

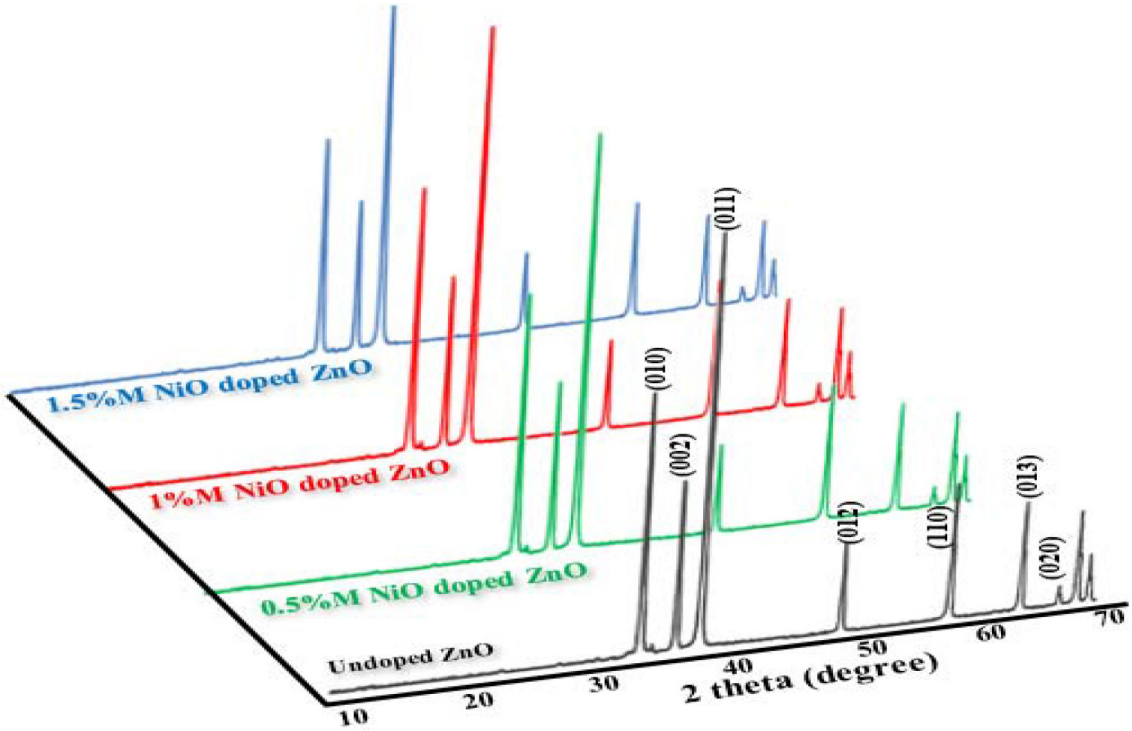

Fig. 7. Powder XRD of nickel doped ZnO nanoparticles.

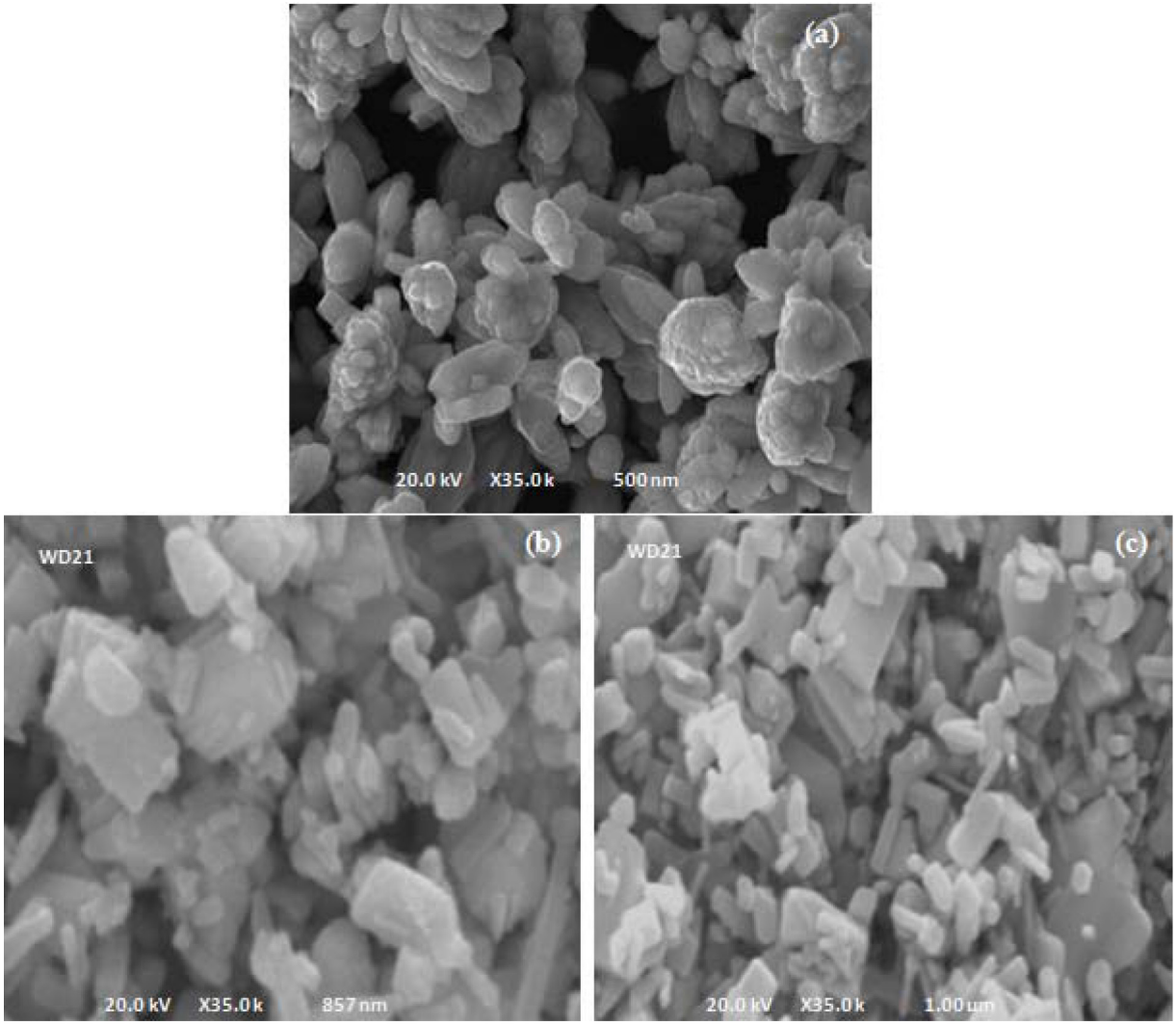

Fig. 8. Characteristic SEM images of a) 0.5 and b) 1.5 M% Ni doped ZnO nanoparticles.

red used with raising of Ni concentration. As well as, lattice structures of particles were more defects and deformed [58].

3.2.3. FTIR analysis

The potential of adding functional groups on the surface of Ni doped ZnO nanoparticles was studied using FTIR analysis. Appearance of new peaks on the surface of the Ni doped ZnO nanoparticles could be attributed to the existence of the surface modifier added and dopant used (Fig. 9). Appearance of the additional peak at 550 cm^{-1} is attributed to the adding nickel as dopant into the lattice of Ni doped ZnO nanoparticles have sharper peaks [59]. The peaks at 420 cm^{-1} and 430 cm^{-1} can be assigned to combined absorption of Zn–O and Ni–O bonds [57]. Moreover, Ni^{2+} occupation at Zn^{2+} sites has been revealed at the 670 and 100 cm^{-1} [60]. The peaks related to adsorbed water on the Ni doped ZnO catalyst was appearance around 1700 cm^{-1}. Furthermore, peaks at the near 3500 cm^{-1} is corresponded to the O–H stretching vibration of hydroxyl groups on the nanoparticles [54]. Kanade et al. reported that peaks at 1638 and 3695 cm^{-1} belong to C=O [61].

3.3. Experimental results

3.3.1. The effect of nanoparticles type on dye degradation

The performance of ZnO doped nickel oxide (0.5% M) was better than the other two types (1% M; 1.5% M) under both sunlight and ultraviolet light (Fig. 10). It was due to the high absorption of light photons by this type of nanoparticles in comparison with other two types (1% M; 1.5% M ZnO: NiO), which could not be due to the decline of energy gap in these types of nanoparticles rather than other two types according to increases the ability of light absorbance in term of decreasing the energy gap [62]. Shahmoradi et al., studied the effect of manganese doped ZnO. Their results indicated that ZnO particles could not absorb at wavelengths more than 400 nm. While the absorption was considerably increased in the presence of doped ZnO with manganese resulting the decreases of energy gap and overlaps the conduction band and valence band of doped ZnO nanoparticles with manganese [63]. Xue and Zou investigated uniform distribution of ZnO nanoparticles on the surface of grpahene. They found the combine of ZnO/grpahene able larger absorptivity of methylene blue com-

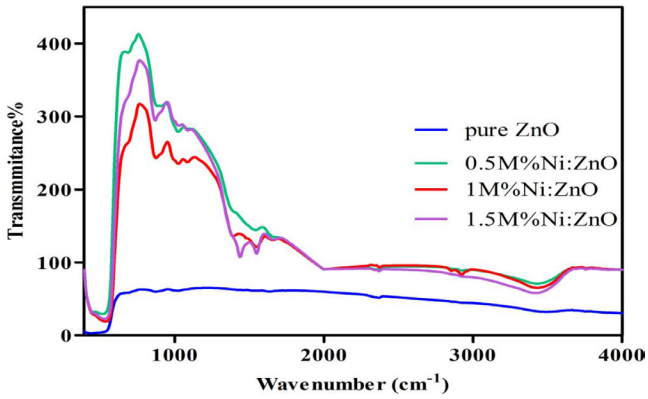

Fig. 9. FTIR of undoped and Ni doped ZnO nanoparticles.

pared pristine ZnO because of the large two-dimensional planar structures of grpahene nanosheets [64].

3.3.2. Effect of nanoparticles dosage on dye decomposition

Assessing the effect of nanoparticles dose on dye removal efficiency showed that the removal efficiency of dye was increased to 67% and 87% under sunlight and UV light illumination as the dosage of nanoparticles changed from 0.2 to 0.8 g/l (Fig. 11). Because, increasing the catalyst dose, more dye molecules are absorbed on the catalyst' surface. On the other hands, the irradiation area increased due to catalyst particles which leads to more generation of Reactive oxygen species (ROS) [65].

Increase of catalyst dosage from 0.8 g/l lead to decrease of removal efficiency due to shadow effect. Because turbidity of the solutions heightened and thus the light penetration into the colored suspension for the photocatalytic stimulation. In fact, light penetration in highly transparent solution is more; on the other hand, increasing the dosage of nanoparticles beyond 0.8 g/l resulted in decreasing the penetration rate of light, which in turn decreased the optical dispersion. Also, increasing nanoparticle dose from 0.8 to 1.2 g/l resulted in dye removal efficiency confers the sta-

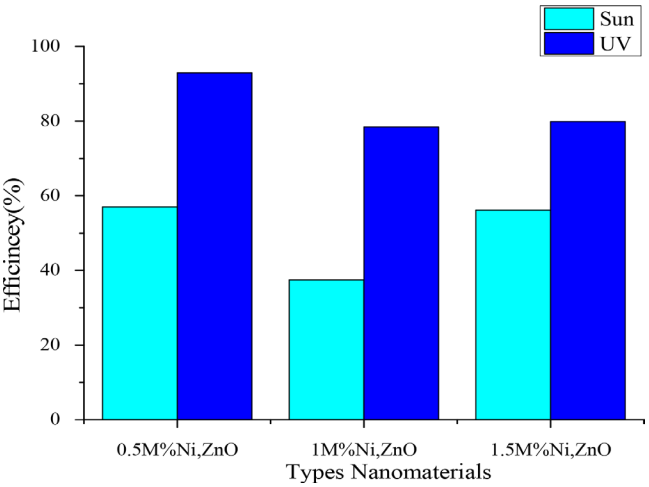

Fig. 10. Average removal efficiency of AO7 dye with nanoparticle dosage of 0.5 g/l, at pH = 5, initial dye concentration of 60 mg/l with different types of nanomaterial.

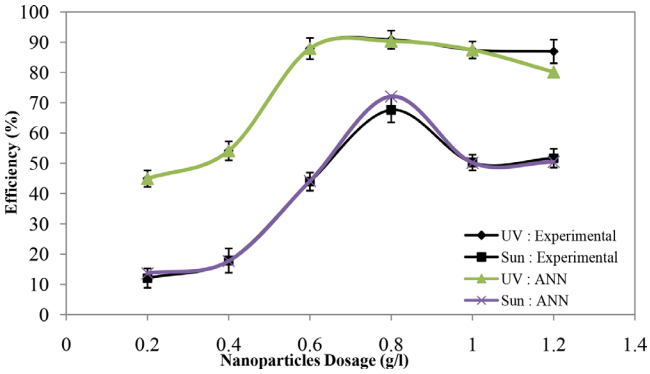

Fig. 11. Average removal efficiency of AO7 dye with different nanoparticle dosage (g/l), an initial dye concentration of 60 mg/l at pH = 5.

bility or decreasing the trend of removal efficiency as the turbidity of the solution would increase with the increase of the nanoparticles dosage [66]. The results were comparable to that of other studies. Maleki and Shahmoradi (2012) assessing feasibility of iron doped ZnO nanoparticle (0.4–1 g/l) to remove direct blue 71 dye, found that the turbidity of the solution increased and the light penetration and removal efficiency decreased *i* when the applied nanoparticles dosage was increased [18]. Moradi et al. (2017) studied the effect of catalyst dose on the AO7 removal in the catalyst doses (Ag–ZnO/CNT) of 0.75 to 2 g/l; they reported that the highest removal rate was about to 100% corresponding to the nanoparticles dose of 1.5 g/l and after that reduced to 97% for 2 g/l [67].

3.3.3 Effect of detention time on nanoparticles performance

The effect of detention time showed that the removal efficiency increases with increases in the detention time with an ascending trend up to 60 min under sunlight and UV illumination, but under UV illumination that ascending trend was more intense in the first 60 min relative to the time interval of 60–90 min (Fig. 12). This could be due to the dispersion and further stimulation of nanoparticle surfaces during the above mentioned time under UV light in comparison with sunlight illumination. Also, other reason could be owing to the penetration and high stimulation of nanoparticles by ultraviolet lamps rather than the sun light

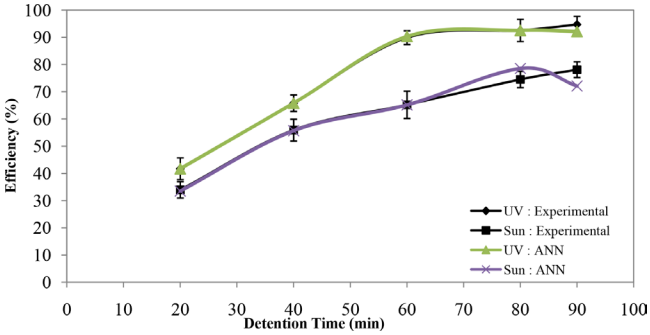

Fig. 12. Average removal efficiency of AO7 dye at pH = 5 and nanoparticle dosage of 0.8 g/l, with an initial dye concentration of 60 mg/l, at different detention time.

in this range of time, at first due to the high gradient of the dye concentration and the availability of more attractive sites, which elevate the transfer rate of dye molecules from aqueous solution to the catalyst surface [68]. Ghalebizade and Ayati (2016) investigated impact of detention time on the removal of AO7 using ZnO/TiO_2 nanocomposite coated on stainless steel electrode [69]. Also, Moradi et al. (2017) studied the effect of detention time on the removal of AO7 using Ag–ZnO/CNT nanoparticles [67]. In both researches, with increase in the detention time, the removal efficiency increased as well.

3.3.4. Effect of pH on nanoparticles performance

Studying the effect of various pH values on nanoparticles performance showed that with increasing pH from 2 to 6, the removal trend was increasing, afterward it was constant up to pH of 10 and descended for pH above 10 (Fig. 13). At the pH more than 10, electron reduction changes in ZnO nanoparticles become evident [40]. Dropping the removal rate in acidic pH is the result of decreasing the hydroxyl radicals concentration. The concentrations of hydroxyl radical increases due to increase in the pH value, which leads to increase in the decomposition of the dye. It can be stated that in alkaline pH, the removal rate of dyes goes even higher. In acidic pH, H^+ ions are competitive with dye ions to be adsorbed by the catalyst surface, consequently dye degradation would decrease [70,71]. Since a AO7 has a sulfonic group in its structure in low pH, the AO7 surface is negatively charged and at the pH is less than 6, ZnO is positively charged, so the dye adheres to the surface of the nanoparticle and the AO7 removal efficiency is reduced [69].

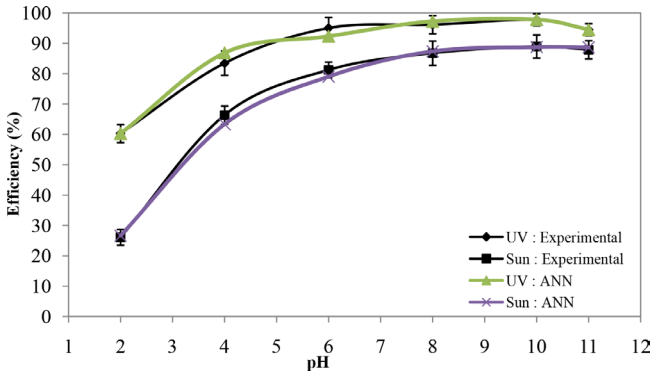

Fig. 13. Average removal efficiency of AO7 dye with a nanoparticle dosage of 0.8 g/l, with an initial dye concentration of 60 mg/l, at different pH level.

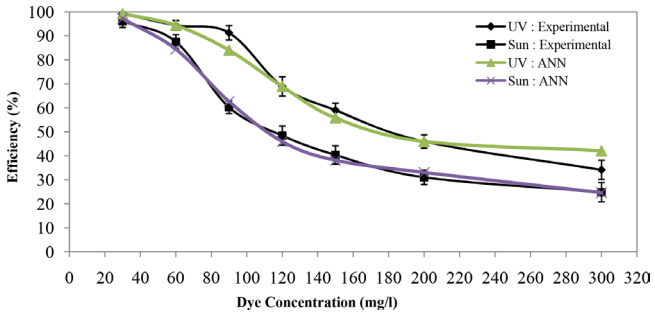

Fig. 14. Average removal efficiency of different concentration of AO7 dye with nanoparticle dosage of 0.8 g/l, at pH =7.

Daneshvar et al. studied the AO7 (20 mg/l) removal by ZnO (160 mg/l); they concluded that the maximum removal efficiency occurs at pH = 7, while at alkaline pH = 9.8, the removal rate was higher than that of acidic pH because ZnO is insoluble at alkaline pH (pH > 10) and forms Zn^+ ion with no photocatalytic properties [40]. In fact, the Zero flux point of ZnO and AO7 dye were 10 and 8.86, respectively, which are close together, because the sun light penetration is lower rather than the UV lamp and the produced hydroxyl radicals were lower in this pH range so the optical dispersion in pH = 2 has decreased under sunlight illumination.

3.3.5. The effect of dye concentration on nanoparticles performance

With an increase in the concentration of AO7 dye, the removal efficiency decreases (Fig. 14). However, the actual amount of dye destruction increased in term of unit mass of nanoparticles so that the initial concentration of dye increased from 30 to 300 mg/l. As a result, the removal efficiency under sunlight and UV irradiation drops from 98 and 99 to 24 and 33% respectively. This is so while the dye removal rate at an equilibrium state rises from 36 and 37 to 93 and 124 mg/l under the sun and UV light, respectively (nanoparticle dose = 0.8 g/l). On the catalyst surface, the decomposition rate of dye was associated with the reaction of the radicals with dye molecules with the formation of hydroxyl radicals. Moreover, with further increases of dye concentration, its degradation efficiency will decrease. In high dye concentrations, the active sites of the catalyst are covered with dye molecules, which prevent from the efficient reaction of hydroxyl radicals and electron holes with dye molecules [72,73]. In addition, with increasing initial concentration of dye, byproducts formation increases owing to the decomposition of dye material and therefore a competition on degradation occurs between this byproduct and dye molecules [74–78]. In fact, It can be stated that with increase in the initial concentration of dye, the probability of reactions between the dye molecules and a variety of oxidizing is increased, which leads to increase in the bleaching rate. In turn, with increase in the dye concentration, the dye degradation performance decreases [79]. At high color concentrations, the catalyst active sites are coated with the dye molecules, which prevent the direct and effective reaction of electron holes and hydroxyl radicals with dye molecules. Nevertheless, increase in the concentration of color, the dye molecules can absorb more light than the catalyst or actually the dye molecules cause UV-screening [76,80].

4. Conclusion

In this work, the removal of AO7 under sunlight and UV light was successfully accomplished. By increasing the catalyst amount above a certain level, the dye removal rate decreased due to the reduced light penetration. The optimum dose was considered as 0.8 g/l of nanoparticle over a detention time of 90 min. Moreover, neutral pH = 7 was obtained as the optimum pH in removing AO7, which is

economically efficient. According to the obtained results, the synthesized nanoparticles are very effective in removing colored wastewater in comparison with un-doped ZnO. Doped ZnO with a suitable metal such as nickel oxide can reduce the energy gap of nanoparticles and thus increase the tendency of these nanoparticles to use sunlight for photocataltic degradation of pollutants. Using visible light rather than UV light, at large scale, is more economical and generates less operational problems. The characterization results indicated that the morphology and crystal structure of nanoparticles has been well preserved. The performance of nanoparticles to remove AO7 under sunlight and UV illumination showed that these nanoparticles potentially use sunlight for degradation pollutants similar to UV light. Thus, it could be concluded that the synthesised nanoparticles could be used to remove various environmental pollutants such as organic pollutants and textile waste waters.

Furthermore, an effort has been made to model the process using artificial neural network approach. Based on the ANN results, the determination of coefficient for sunlight and ultraviolet irradiation was 0.991 and 0.981, respectively and this results demonstrates that the ANN model fits the experimental data and thus, it can be further used to generate useful predictions.

Acknowledgment

The authors wish to acknowledge the financial support of carrying out this project (Grant Number: 92024) from Kermanshah University of Medical Sciences.

References

[1] A. Asghar, A.A.A. Raman, W.M.A.W. Daud, Advanced oxidation processes for in-situ production of hydrogen peroxide/hydroxyl radical for textile wastewater treatment: a review, J. Clean. Prod., 87 (2015) 826–838.
[2] D. Mostafa, Waste water treatment in textile industries - the concept and current removal technologies, J. Bio. Env. Sci., 7 (2015) 501–525.
[3] Y. Vasseghian, E.-N. Dragoi, Modeling and optimization of acid blue 193 removal by UV and peroxydisulfate process, J. Environ. Eng., 144 (2018) 06018003.
[4] E. Deletze, A. Antoniadis, V. Kitsiou, E. Kostopoulou, D. Lutic, I. Cretescu, I. Poulios, Photocatalytic treatment of colored wastewater from medical laboratories: photodegradation of Nuclear Fast Red, Desal. Water Treat., 57 (2016) 18897–18905.
[5] W. Bunmahotama, W.-N. Hung, T.-F. Lin, Simulation of the adsorption capacity of polar organic compounds and dyes from water onto activated carbons: Model development and validation, Sustain. Environ. Res., 28 (2018) 57–64.
[6] B. Mi, M. Hu, Layer-by-layer assembly of graphene oxide membranes via electrostatic interaction and eludication of water and solute transport mechanisms, in, Google Patents, 2018.
[7] C. Tang, H. Bai, L. Liu, X. Zan, P. Gao, D.D. Sun, W. Yan, A green approach assembled multi-functional Ag/AgBr/TNF membrane for clean water production & disinfection of bacteria through utilizing visible light, Appl. Catal. B- Environ., 196 (2016) 57–67.
[8] H. Sun, J. Jiang, Y. Xiao, J. Du, Efficient removal of polycyclic aromatic hydrocarbons, dyes, and heavy metal ions by a homopolymer vesicle, ACS Appl. Mater. Interfaces, 10 (2017) 713–722.
[9] M. Hadi, G. McKay, M.R. Samarghandi, A. Maleki, M.S. Aminabad, Prediction of optimum adsorption isotherm: comparison of chi-square and Log-likelihood statistics, Desal. Water Treat., 49 (2012) 81–94.
[10] R. Rezaee, A. Maleki, A. Jafari, S. Mazloomi, Y. Zandsalimi, A.H. Mahvi, Application of response surface methodology for optimization of natural organic matter degradation by UV/H_2O_2 advanced oxidation process, J. Environ. Healt. Sci. Eng., 12 (2014) 67.
[11] S. Mondal, M.K. Purkait, S. De, Advances in dye removal technologies, Springer, 2018.
[12] A. Shokri, K. Mahanpoor, Using UV/ZnO process for degradation of Acid red 283 in synthetic wastewater, Bulg. Chem. Commun., 50 (2018) 27–32.
[13] T. Mousavand, S. Ohara, M. Umetsu, J. Zhang, S. Takami, T. Naka, T. Adschiri, Hydrothermal synthesis and in situ surface modification of boehmite nanoparticles in supercritical water, J. Supercrit. Fluids, 40 (2007) 397–401.
[14] S. Teixeira, P. Martins, S. Lanceros-Méndez, K. Kühn, G. Cuniberti, Re-usability of photocatalytic TiO_2 and ZnO nanoparticles immobilized in poly (vinylidene difluoride)-co-trifluoroethylene, Appl. Surf. Sci., 384 (2016) 497–504.
[15] J. Gómez-Pastora, S. Dominguez, E. Bringas, M.J. Rivero, I. Ortiz, D.D. Dionysiou, Review and perspectives on the use of magnetic nanophotocatalysts (MNPCs) in water treatment, Chem. Eng. J., 310 (2017) 407–427.
[16] D.N. Yadav, K.A. Kishore, B. Bethi, S.H. Sonawane, D. Bhagawan, ZnO nanophotocatalysts coupled with ceramic membrane method for treatment of Rhodamine-B dye waste water, Environ. Dev. Sustain., (2017) 1–14.
[17] R. Ameta, M.S. Solanki, S. Benjamin, S.C. Ameta, Chapter 6 - photocatalysis, in: advanced oxidation processes for waste water treatment, Academic Press, 2018, pp. 135–175.
[18] A. Maleki, B. Shahmoradi, Solar degradation of direct blue 71 using surface modified iron doped ZnO hybrid nanomaterials, Water. Sci. Tech., 65 (2012) 1923–1928.
[19] F. Achouri, S. Corbel, L. Balan, K. Mozet, E. Girot, G. Medjahdi, M.B. Said, A. Ghrabi, R. Schneider, Porous Mn-doped ZnO nanoparticles for enhanced solar and visible light photocatalysis, Mater. Des., 101 (2016) 309–316.
[20] Z. Zhang, C. Shao, X. Li, C. Wang, M. Zhang, Y. Liu, Electro spun nanofibers of p-type NiO/n-type ZnO heterojunctions with enhanced photoc atalytic activity, ACS Appl. Mater. Interfaces, 2 (2010) 2915–2923.
[21] P.G. Ramos, E. Flores, L.A. Sánchez, R.J. Candal, M. Hojamberdiev, W. Estrada, J. Rodriguez, Enhanced photoelectrochemical performance and photocatalytic activity of ZnO/TiO_2 nanostructures fabricated by an electro statically modified electro spinning, Appl. Surf. Sci., 426 (2017) 844–851.
[22] N. Krstulović, K. Salamon, O. Budimlija, J. Kovač, J. Dasović, P. Umek, I. Capan, Parameters optimization for synthesis of Al-doped ZnO nanoparticles by laser ablation in water, Appl. Surf. Sci., 440 (2018) 916–925.
[23] F. Ajala, A. Hamrouni, A. Houas, H. Lachheb, B. Megna, L. Palmisano, F. Parrino, The influence of Al doping on the photocatalytic activity of nanostructured ZnO: The role of adsorbed water, Appl. Surf. Sci., 445 (2018) 376–382.
[24] O. Bechambi, M. Chalbi, W. Najjar, S. Sayadi, Photocatalytic activity of ZnO doped with Ag on the degradation of endocrine disrupting under UV irradiation and the investigation of its antibacterial activity, Appl. Surf. Sci., 347 (2015) 414–420.
[25] B. Sarma, B.K. Sarma, Fabrication of Ag/ZnO heterostructure and the role of surface coverage of ZnO micro rods by Ag nanoparticles on the photophysical and photocatalytic properties of the metal-semiconductor system, Appl. Surf. Sci., 410 (2017) 557–565.
[26] Y.-C. Chang, C.-C. Hsu, S.-H. Wu, K.-W. Chuang, Y.-F. Chen, Fabrication of Cu-doped ZnO nanoneedles on different substrate via wet chemical approach: Structural characterization and photocatalytic performance, Appl. Surf. Sci., 447 (2018) 213–221.
[27] S. Safa, S. Mokhtari, A. Khayatian, R. Azimirad, Improving ultraviolet photodetection of ZnO nanorods by Cr doped ZnO encapsulation process, Opt. Commun., 413 (2018) 131–135.

[28] N.A. Putri, V. Fauzia, S. Iwan, L. Roza, A.A. Umar, S. Budi, Mn-doping-induced photocatalytic activity enhancement of ZnO nanorods prepared on glass substrates, Appl. Surf. Sci., 439 (2018) 285–297.
[29] L.M. Trinca, A.C. Galca, A.G. Boni, M. Botea, L. Pintilie, Effect of Li doping on the electric and pyroelectric properties of ZnO thin films, Appl. Surf. Sci., 427 (2018) 29–37.
[30] S. Bhatia, N. Verma, R.K. Bedi, Corrigendum to "Sn-doped ZnO nanopetal networks for efficient photocatalytic degradation of dye and gas sensing applications", Appl. Surf. Sci., 407 (2017) 495–502], Appl. Surf. Sci., 441 (2018) 1086.
[31] R. Beura, R. Pachaiappan, P. Thangadurai, A detailed study on Sn^{4+} doped ZnO for enhanced photocatalytic degradation, Appl. Surf. Sci., 433 (2018) 887–898.
[32] E. Alizadeh, H. Baseri, Catalytic degradation of Amlodipine Besylate using ZnO, Cu doped ZnO, and Fe doped ZnO nanoparticles from an aqueous solution: Investigating the effect of different parameters on degradation efficiency, Solid State Sci., 78 (2018) 86–94.
[33] S. Fabbiyola, V. Sailaja, L.J. Kennedy, M. Bououdina, J.J. Vijaya, Optical and magnetic properties of Ni-doped ZnO nanoparticles, J. Alloys Compd., 694 (2017) 522–531.
[34] B. Shahmoradi, I. Ibrahim, K. Namratha, N. Sakamoto, S. Ananda, R. Somashekar, K. Byrappa, Surface modification of indium doped ZnO hybrid nanoparticles with n-butylamine, Int. J. Chem. Eng. Res., 2 (2010) 107–117.
[35] A. Sharma, M. Verma, A. Haritash, Photocatalytic degradation of Acid Orange 7 (AO7) dye using TiO_2, Int. J. Eng. Res. Technol. (RACEE 2015Conference Proceedings), 4 (2015) 34–36.
[36] F. Han, V. Kambala, R. Dharmarajan, Y. Liu, R. Naidu, Photocatalytic degradation of azo dye acid orange 7 using different light sources over Fe^{3+}-doped TiO_2 nanocatalysts, Environ. Technol. Innovation, 12 (2018) 27–42.
[37] E.H. Umukoro, S.S. Madyibi, M.G. Peleyeju, L. Tshwenya, E.H. Viljoen, J.C. Ngila, O.A. Arotiba, Photocatalytic application of Pd-ZnO-exfoliated graphite nanocomposite for the enhanced removal of acid orange 7 dye in water, Solid State Sci., 74 (2017) 118–124.
[38] A. Khani, M.R. Sohrabi, Simultaneous synthesis-immobilization of nano ZnO on perlite for photocatalytic degradation of an azo dye in semi batch packed bed photoreactor, Pol. J. Chem. Technol., 14 (2012) 69–76.
[39] H. Akhlaghi, Photocatalytic degradation for acid orange 7 using zinc oxide nanostructure prepared with activated carbon, Anal. Chem. Lett., 3 (2013) 65–69.
[40] N. Daneshvar, M. Rasoulifard, A. Khataee, F. Hosseinzadeh, Removal of CI acid orange 7 from aqueous solution by UV irradiation in the presence of ZnO nanopowder, J. Hazard. Mater., 143 (2007) 95–101.
[41] C. Cheng, G. Xu, H. Zhang, Y. Luo, Hydrothermal synthesis Ni-doped ZnO nanorods with room-temperature ferromagnetism, Mater. Lett., 62 (2008) 1617–1620.
[42] M. Pirsaheb, B. Shahmoradi, M. Beikmohammadi, E. Azizi, H. Hossini, G.M. Ashraf, Photocatalytic degradation of Aniline from aqueous solutions under sunlight illumination using immobilized Cr: ZnO nanoparticles, Sci. Rep., 7 (2017) 1473.
[43] W.-E. Thung, S.-A. Ong, L.-N. Ho, Y.-S. Wong, F. Ridwan, H.K. Lehl, Y.-L. Oon, Y.-S. Oon, Biodegradation of acid orange 7 in a combined anaerobic-aerobic up-flow membrane-less microbial fuel cell: Mechanism of biodegradation and electron transfer, Chem. Eng. J., 336 (2018) 397–405.
[44] The Math Works Inc., Natick, MA, in, 2012.
[45] S.T. Bararpour, M.R. Feylizadeh, A. Delparish, M. Qanbarzadeh, M. Raeiszadeh, M. Feilizadeh, Investigation of 2-nitrophenol solar degradation in the simultaneous presence of $K_2S_2O_8$ and H_2O_2: Using experimental design and artificial neural network, J. Clean. Prod., 176 (2018) 1154–1162.
[46] M.E. López, E.R. Rene, Z. Boger, M.C. Veiga, C. Kennes, Modelling the removal of volatile pollutants under transient conditions in a two-stage bioreactor using artificial neural networks, J. Hazard. Mater., 324 (2017) 100–109.
[47] M. Moghri, E.N. Dragoi, A. Salehabadi, D.K. Shukla, Y. Vasseghian, Effect of various formulation ingredients on thermal characteristics of PVC/clay nanocomposite foams: experimental and modeling, e-Polym., 17 (2017) 119–128.
[48] D.S. Badkar, K.S. Pandey, G. Buvanashekaran, Development of RSM-and ANN-based models to predict and analyze the effects of process parameters of laser-hardened commercially pure titanium on heat input and tensile strength, Int. J. Adv. Manuf. Tech., 65 (2013) 1319–1338.
[49] Y. Vasseghian, M. Ahmadi, M. Joshaghani, Simultaneous ash and sulphur removal from bitumen using column flotation technique: Experiments, RSM modeling and optimization, Phys. Chem. Res., 5 (2017) 195–204.
[50] S. Ghoreishi, E. Heidari, Extraction of epigallocatechin-3-gallate from green tea via supercritical fluid technology: neural network modeling and response surface optimization, J. Supercrit. Fluids, 74 (2013) 128–136.
[51] Y. Vasseghian, M. Ahmadi, M. Joshaghani, Ultrasound assisted ash and sulphur removal from bitumen using column flotation technique: Experimental, RSM and ANN methods in modelling and optimization of process, Iran. J. Sci. Technol., Trans. A: Sci., 41 (2017) 1149–1163.
[52] A. Esmaeili, E. Hejazi, Y. Vasseghian, Comparison study of biosorption and coagulation/air flotation methods for chromium removal from wastewater: experiments and neural network modeling, RSC Adv., 5 (2015) 91776–91784.
[53] G. Huang, J. Wang, X. Zhong, G. Zhou, H. Yan, Synthesis, structure, and room-temperature ferromagnetism of Ni-doped ZnO nanoparticles, J. Mater. Sci., 42 (2007) 6464–6468.
[54] Y. Wang, T. Liu, Q. Huang, C. Wu, D. Shan, Synthesis and their photocatalytic properties of Ni-doped ZnO hollow micro spheres, J. Mater. Res., 31 (2016) 2317–2328.
[55] P. Pascariu, I.V. Tudose, M. Suchea, E. Koudoumas, N. Fifere, A. Airinei, Preparation and characterization of Ni, Co doped ZnO nanoparticles for photocatalytic applications, Appl. Surf. Sci., 448 (2018) 481–488.
[56] H. Liu, J. Yang, Z. Hua, Y. Zhang, L. Yang, L. Xiao, Z. Xie, The structure and magnetic properties of Cu-doped ZnO prepared by sol–gel method, Appl. Surf. Sci., 256 (2010) 4162–4165.
[57] E. Sherly, J.J. Vijaya, L.J. Kennedy, B. Sreedhar, NiO coupled ZnO nanoparticles: preparation, characterization and their UV-vis photocatalytic activities, J. Nanosci. Nanotechnol., 16 (2016) 9784–9793.
[58] Y. Mao, Y. Cheng, J. Wang, H. Yang, M. Li, J. Chen, M. Chao, Y. Tong, E. Liang, Amorphous NiO electro catalyst over coated ZnO nanorod photoanodes for enhanced photoelectrochemical performance, New J. Chem., 40 (2016) 107–112.
[59] R. Elilarassi, G. Chandrasekaran, Synthesis, structural and optical characterization of Ni-doped ZnO nanoparticles, J. Mater. Sci.: Mater. Electron., 22 (2011) 751–756.
[60] K. Raja, P. Ramesh, D. Geetha, Synthesis, structural and optical properties of ZnO and Ni-doped ZnO hexagonal nanorods by Co-precipitation method, Spectrochim. Acta, Part A, 120 (2014) 19–24.
[61] K.G. Kanade, B.B. Kale, J.-O. Baeg, S.M. Lee, C.W. Lee, S.-J. Moon, H. Chang, Self-assembled aligned Cu doped ZnO nanoparticles for photocatalytic hydrogen production under visible light irradiation, Mater. Chem. Phys., 102 (2007) 98–104.
[62] A. Maleki, M. Safari, B. Shahmoradi, Y. Zandsalimi, H. Daraei, F. Gharibi, Photocatalytic degradation of humic substances in aqueous solution using Cu-doped ZnO nanoparticles under natural sunlight irradiation, Environ. Sci. Pollut. Res., 22 (2015) 16875–16880.
[63] B. Shahmoradi, K. Namratha, K. Byrappa, K. Soga, S. Ananda, R. Somashekar, Enhancement of the photocatalytic activity of modified ZnO nanoparticles with manganese additive, Res. Chem. Intermed., 37 (2011) 329–340.
[64] B. Xue, Y. Zou, Uniform distribution of ZnO nanoparticles on the surface of grpahene and its enhanced photocatalytic performance, Appl. Surf. Sci., 440 (2018) 1123–1129.
[65] A. Jonidi-Jafari, M. Gholami, M. Farzadkia, A. Esrafili, M. Shirzad-Siboni, Application of Ni-doped ZnO nanorods for degradation of diazinon: Kinetics and by-products, Sep. Sci. Technol., 52 (2017) 2395–2406.

[66] A. Maleki, M. Safari, R. Rezaee, R.D.C. Soltani, B. Shahmoradi, Y. Zandsalimi, Photocatalytic degradation of humic substances in the presence of ZnO nanoparticles immobilized on glass plates under ultraviolet irradiation, Sep. Sci. Technol., 51 (2016) 2484–2489.
[67] M. Moradi, M. Haghighi, S. Allahyari, Precipitation dispersion of Ag–ZnO nanocatalyst over functionalized multi wall carbon nanotube used in degradation of Acid Orange from wastewater, Process Saf. Environ. Prot., 107 (2017) 414–427.
[68] M. Safari, A. Khataee, R.D.C. Soltani, R. Rezaee, Ultrasonically facilitated adsorption of an azo dye onto nanostructures obtained from cellulosic wastes of broom and cooler straw, J. Colloid Interface Sci., 522 (2018) 228–241.
[69] M. Ghalebizade, B. Ayati, Solar photoelectro catalytic degradation of Acid Orange 7 with ZnO/TiO_2 nanocomposite coated on stainless steel electrode, Process Saf. Environ. Prot., 103 (2016) 192–202.
[70] C. Chen, C. Lu, Y. Chung, J. Jan, UV light induced photodegradation of malachite green on TiO_2 nanoparticles, J. Hazard. Mater., 141 (2007) 520–528.
[71] B. Krishnakumar, B. Subash, M. Swaminathan, AgBr–ZnO–An efficient nano-photocatalyst for the mineralization of Acid Black 1 with UV light, Sep. Purif. Technol., 85 (2012) 35–44.
[72] R.D.C. Soltani, M. Safari, A. Maleki, H. Godini, M.H. Mahmoudian, M.A. Pordel, Application of nanocrystalline iranian diatomite in immobilized form for removal of a textile dye, J. Dispersion Sci. Technol., 37 (2016) 723–732.
[73] B. Shahmoradi, A. Maleki, K. Byrappa, Removal of Disperse Orange 25 using in situ surface-modified iron-doped TiO_2 nanoparticles, Desal. Water Treat., 53 (2015) 3615–3622.
[74] K. Hayat, M. Gondal, M.M. Khaled, S. Ahmed, A.M. Shemsi, Nano ZnO synthesis by modified sol gel method and its application in heterogeneous photocatalytic removal of phenol from water, Appl. Catal., A, 393 (2011) 122–129.
[75] M. Mahalakshmi, B. Arabindoo, M. Palanichamy, V. Murugesan, Photocatalytic degradation of carbofuran using semiconductor oxides, J. Hazard. Mater., 143 (2007) 240–245.
[76] J. Wu, H. Zhang, J. Qiu, Degradation of acid orange 7 in aqueous solution by a novel electro/Fe^{2+}/peroxydisulfate process, J. Hazard. Mater., 215 (2012) 138–145.
[77] B. Shahmoradi, M. Negahdary, A. Maleki, Hydrothermal synthesis of surface-modified, manganese-doped TiO_2 nanoparticles for photodegradation of methylene blue, Environ. Eng. Sci., 29 (2012) 1032–1037.
[78] B. Shahmoradi, A. Maleki, K. Byrappa, Photocatalytic degradation of amaranth and brilliant blue FCF dyes using in situ modified tungsten doped TiO_2 hybrid nanoparticles, Catal. Sci. Technol., 1 (2011) 1216–1223.
[79] H. Daraei, A. Maleki, A.H. Mahvi, Y. Zandsalimi, L. Alaei, F. Gharibi, Synthesis of ZnO nano-sono-catalyst for degradation of reactive dye focusing on energy consumption: operational parameters influence, modeling, and optimization, Desal. Water Treat., 52 (2014) 6745–6755.
[80] G. Li, J. Qu, X. Zhang, J. Ge, Electrochemically assisted photocatalytic degradation of Acid Orange 7 with β-PbO_2 electrodes modified by TiO_2, Water Res., 40 (2006) 213–220.